Charmonia production in pp collisions under NRQCD formalism

Vineet Kumar[1,2] and Prashant Shukla[1,2,*]

[1] *Nuclear Physics Division, Bhabha Atomic Research Center, Mumbai, India*

[2] *Homi Bhabha National Institute, Anushakti Nagar, Mumbai, India*

(Dated: February 10, 2016)

Abstract

We calculate the high p_T quarkonia production using NRQCD method. In NRQCD formalism quarkonia cross-section can be written as a product of short distance QCD cross-sections and long distance matrix elements (LDMEs). We use measured data of ψ(2S), χ_c and J/ψ at 1.8, 1.96, 7 and 8 TeV to constrin LDMEs. These LDMEs are then used to calculate charmonia cross-section at 13 and 14 TeV.

PACS numbers: 12.38.Mh, 24.85.+p, 25.75.-q

Keywords: quark-gluon plasma, quarkonia, suppression, regeneration

* pshukla@barc.gov.in

I. INTRODUCTION

Heavy-ion collisions at relativistic energies are performed to create and characterize quark gluon plasma (QGP), a phase of strongly-interacting matter at high energy density where quarks and gluons are no longer bound within hadrons. The quarkonia states (J/ψ and Υ) have been some of the most popular tools since their suppression was proposed as a signal of QGP formation [1]. The understanding of these probes has evolved substantially via measurements through three generations of experiments: the SPS (at CERN), RHIC (at BNL) and the LHC (at CERN) and by a great deal of theoretical activity. (For recent reviews see Refs. [2–4].) Quarkonia are produced early in the heavy-ion collisions and, if they evolve through the deconfined medium, their yields should be suppressed in comparison with those in pp collisions.

To be written .....

II. QUARKONIA PRODUCTION IN P+P COLLISIONS

In this section we describe the production of quarkonia at high transverse momenta in p+p collisions. The factorization formalism of the NRQCD provides a theoretical framework for studying the heavy quarkonium production and decay. Under NRQCD the cross-section for direct production of a resonance ψ in pp collision can be expressed in factorized form. The dominant processes in evaluating the differential yields of heavy mesons as a function of p_T are the $2 \to 2$ processes of the kind $g + q \to \psi + q$, $q + \bar{q} \to \psi + g$ and $g + g \to \psi + g$, where ψ refers to the heavy meson. We label the process generically as $a + b \to \psi + X$, where a and b are the light incident partons. The invariant cross-section can be written as

$$E\frac{d^3\sigma^\psi}{d^3p} = \sum_{a,b} \int\int dx_a\, dx_b G_{a/p}(x_a, \mu_F^2) G_{b/p}(x_b, \mu_F^2) \frac{\hat{s}}{\pi} \frac{d\sigma}{d\hat{t}} \otimes \delta(\hat{s} + \hat{t} + \hat{u} - M^2) \qquad (1)$$

where, $G_{a/p}(G_{b/p})$ is the parton distribution function (PDF) of the incoming parton $a(b)$ in the incident proton, which depends on the momentum fraction $x_a(x_b)$ and the factorization scale μ_F as well as on the renormalization scale μ_R. However, as we have chosen $\mu_F = \mu_R$, in our case PDFs are function of x and μ_F only. The parton level cross-section $\mathrm{d}\sigma/\mathrm{d}\hat{t}$ is defined as

$$\frac{d\sigma}{d\hat{t}} = \frac{d\sigma}{d\hat{t}}(ab \to Q\overline{Q}(^{2S+1}L_J) + X) M_L(Q\overline{Q}(^{2S+1}L_J) \to \psi) \qquad (2)$$

The short distance contribution $d\sigma/d\hat{t}(ab \to Q\overline{Q}(^{2S+1}L_J) + X)$ can be calculated within the framework of perturbative QCD (pQCD). $M_L(Q\overline{Q}(^{2S+1}L_J) \to \psi)$ are the nonperturbative LDMEs and can only be estimated by comparison with experimental measurements. At this stage, the integration upon x_b can be performed using the properties of delta function. To solve the integration we have to express the $\hat{s}$, $\hat{t}$, and $\hat{u}$ in terms of x_a, x_b, resonance transeverse momentum p_T and rapidity y. For $ab \to \psi + X$ kind of processes following are the relations between $\hat{s}$, $\hat{t}$, $\hat{u}$ and meson variables

$$\begin{aligned} \hat{s} &= x_a\, x_b\, s \\ \hat{t} &= M^2 - x_a \sqrt{s}\, m_T\, e^{-y} \\ \hat{u} &= M^2 - x_b \sqrt{s}\, m_T\, e^{y} \end{aligned} \tag{3}$$

Writing down $\hat{s} + \hat{t} + \hat{u} - M^2$ and solving for x_b we obtain

$$x_b = \frac{1}{\sqrt{s}} \frac{x_a \sqrt{s}\, m_T\, e^{-y} - m_H^2}{x_a \sqrt{s} - m_T\, e^{y}}. \tag{4}$$

The double differential cross-section upon p_T and y takes the following form

$$\frac{d^2\sigma^{ab\to cd}}{dp_T\, dy} = \sum_{a,b} \int_{x_a^{min}}^{1} dx_a\, G_{a/A}(x_a,\, \mu_F^2)\, G_{b/B}(x_b,\, \mu_F^2) \times 2p_T \frac{x_a\, x_b}{x_a - \frac{m_T}{\sqrt{s}} e^{y}} \frac{d\sigma}{d\hat{t}}, \tag{5}$$

where, $\sqrt{s}$ being the total energy in the centre-of-mass and y is the rapidity of the $Q\bar{Q}$ pair. The minimum value of x_a is

$$x_{a\min} = \frac{1}{\sqrt{s}} \frac{\sqrt{s}\, m_T\, e^{y} - m_H^2}{\sqrt{s} - m_T\, e^{-y}}. \tag{6}$$

The short distance invariant differential cross-section is given by

$$\frac{d\sigma}{d\hat{t}}(ab \to Q\overline{Q}(^{2S+1}L_J) + X) = \frac{|\mathcal{M}|^2}{16\pi \hat{s}^2}, \tag{7}$$

where $\hat{s}$ and $\hat{t}$ are the parton level Mandelstam variables. $|\mathcal{M}|^2$ is the feynman squared amplitude averaged over initial spin of partons. In our calculations, we used the expressions for the short distance Color Singlet (CS) cross-sections given in Refs. [11–13] and the Color Octet (CO) cross-sections given in Refs. [14–16]. In our numerical computation, we use CTEQ6M [7] for the parton distribution functions.

The LDMEs are predicted to scale with a definite power of the relative velocity v of the heavy constituents inside $Q\bar{Q}$ bound states. In the limit $v << 1$, the production of quarkonium is based on the ${}^3S_1^{[1]}$ and ${}^3P_J^{[1]}$ (J = 0,1,2) CS states and ${}^1S_0^{[8]}$, ${}^3S_1^{[8]}$ and ${}^3P_J^{[8]}$ CO states. The differential cross section for the direct production of J/ψ can be written as the sum of the contributions,

$$\begin{aligned} d\sigma(J/\psi) = {} & d\sigma(Q\bar{Q}([{}^3S_1]_1))M_L(Q\bar{Q}([{}^3S_1]_1) \to J/\psi) + d\sigma(Q\bar{Q}([{}^1S_0]_8))M_L(Q\bar{Q}([{}^1S_0]_8) \to J/\psi) \\ & + d\sigma(Q\bar{Q}([{}^3S_1]_8))M_L(Q\bar{Q}([{}^3S_1]_8) \to J/\psi) + d\sigma(Q\bar{Q}([{}^3P_0]_8))M_L(Q\bar{Q}([{}^3P_0]_8) \to J/\psi) \\ & + d\sigma(Q\bar{Q}([{}^3P_1]_8))M_L(Q\bar{Q}([{}^3P_1]_8) \to J/\psi) + d\sigma(Q\bar{Q}([{}^3P_2]_8))M_L(Q\bar{Q}([{}^3P_2]_8) \to J/\psi) \\ & + \cdots , \end{aligned} \tag{8}$$

where the quantity in the brackets [ ] represents the angular momentum quantum numbers of the $Q\bar{Q}$ pair in the Fock expansion. The subscript on [ ] refers to the color structure of the $Q\bar{Q}$ pair, 1 being the color-singlet and 8 being the color-octet. The dots represent terms which contribute at higher powers of v. The short distance cross sections $d\sigma(Q\bar{Q})$ correspond to the production of a $Q\bar{Q}$ pair in a particular color and spin configuration, while the long distance matrix element $M_L(Q\bar{Q}) \to J/\psi$ corresponds to the probability of the $Q\bar{Q}$ state to convert to the quarkonium wavefunction. This probability includes any necessary prompt emission of soft gluons to prepare a color neutral system that matches onto the corresponding Fock component of the quarkonium wavefunction. Power counting rules tell us that contributions from the color-octet matrix elements in Eq. 8 are suppressed by v^4 compared to the color singlet matrix elements. The case of the p-wave bound states (χ_{c0}, χ_{c1}, and χ_{c2}, sometimes collectively referred to as χ_{cJ}, and the corresponding states of the b quark) is slightly different. The color-singlet state $Q\bar{Q}[{}^3P_J]_1$ and the color-octet state $Q\bar{Q}[{}^3S_1]_8$ contribute to the same order in v (v^5) because of the angular momentum barrier for $p-$wave states, and hence both need to be included for a consistent calculation in v. For the calculation of the production cross section, we consistently take the contributions to the lowest order in v. The χ_c differential cross section can be written as

$$\begin{aligned} d\sigma(\chi_{cJ}) = {} & d\sigma(Q\bar{Q}([{}^3P_J]_1))M_L(Q\bar{Q}([{}^3P_J]_1) \to \chi_{cJ}) + d\sigma(Q\bar{Q}([{}^3S_1]_8))M_L(Q\bar{Q}([{}^3S_1]_8) \to \chi_{cJ}) \\ & + \cdots \end{aligned} \tag{9}$$

Similar expressions hold for the $\chi_b(1P)$, $\chi_b(2P)$ and $\chi_b(3P)$ mesons. Using above mentioned formalism we calculate the cross-section of charmonia states at LHC energies. For J/ψ

production in $p-p$ collisions at LHC energies, three sources need to be considered: direct J/ψ production from initial parton-parton hard scattering, feed-down contributions to the J/ψ from the decay of heavier charmonium states, predominantly from $\psi(2S)$, χ_{c0}, χ_{c1} and χ_{c2} and J/ψ from B hadron decays. The sum of the first two sources is called "prompt J/ψ" and the third source is called "J/ψ from B". On the other hand, $\psi(2S)$ has no significant feed-down contributions from higher mass states. We call this direct contribution as "prompt $\psi(2S)$" to be consistent with the experiments. For the production of prompt J/ψ we consider the direct contribution, and feed-down contributions from $\chi_{c0}(1P)$, $\chi_{c1}(1P)$, $\chi_{c2}(1P)$ and $\psi(2S)$. The relevant branching fractions are given in Table I,

TABLE I. Relevant branching fractions for charmonia [24]

Meson From	to χ_{c0}	to χ_{c1}	to χ_{c2}	to J/ψ
$\psi(2S)$	0.0962	0.092	0.0874	0.595
χ_{c0}				0.0116
χ_{c1}				0.344
χ_{c2}				0.195

In this work, following [14, 15] we use the values of the color-singlet matrix elements calculated using the potential model. The expressions and the values for the color-singlet operators can be found in [14, 15, 17]. The values are obtained by solving the non-relativistic wavefunctions:

$$
\begin{aligned}
&M_L(c\bar{c}([^3S_1]_1) \to J/\psi) = 3M_L(c\bar{c}([^1S_0]_1) \to J/\psi) = 3N_c\frac{|R_{n=1}(0)|^2}{2\pi} = 1.2 \text{ GeV}^3 \ , \\
&M_L(c\bar{c}([^3S_1]_1) \to \psi(2S)) = 3M_L(c\bar{c}([^1S_0]_1) \to \psi(2S)) = 3N_c\frac{|R_{n=2}(0)|^2}{2\pi} = 0.76 \text{ GeV}^3 \ , \\
&\frac{1}{5}M_L(c\bar{c}([^3P_2]_1) \to \chi_{c2}(1P)) = \frac{1}{3}M_L(c\bar{c}([^3P_1]_1) \to \chi_{c1}(1P)) = M_L(c\bar{c}([^3P_0]_1) \to \chi_{c0}(1P)) \\
&= 3N_c\frac{|R'_{n=1}(0)|^2}{2\pi} = 0.054 m^2_{\text{charm}} \text{ GeV}^3
\end{aligned}
\tag{10}
$$

here $R(0)$ is the radial wavefunction at the origin, $R'(0)$ is the first derivative of the radial wavefunction at the origin, and n refers to the radial quantum number. We take the mass of the charm quark, $m_{\text{charm}} = 1.6$ GeV.

The color-octet operators can not be related to the non-relativistic wavefunctions of $Q\bar{Q}$ since it involves a higher Fock state. We used measured data from LHC [8–10] and TeVatron [22] to constrain these Color Octet Matrix elements. For the net production of J/ψ we consider the direct contribution, and feed-down contributions from $\chi_{c0}(1P)$, $\chi_{c1}(1P)$, $\chi_{c2}(1P)$ and $\psi(2S)$. Yields of $\psi(2S)$ have been measured at TeVatron [23] and LHC [8]. Data for χ_{cJ} is available from TeVatron [23].

The following color-singlet and color-octet contributions are relevant for our calculation.

1. Direct contributions

$$\begin{aligned}
&M_L(c\bar{c}([^3S_1]_1) \to J/\psi) = 1.2\,\mathrm{GeV}^3 \\
&M_L(c\bar{c}([^3S_1]_8) \to J/\psi) \\
&M_L(c\bar{c}([^1S_0]_8) \to J/\psi) \\
&M_L(c\bar{c}([^3P_0]_8) \to J/\psi)
\end{aligned} \tag{11}$$

2. Feed-down contribution from $\psi(2S)$

$$\begin{aligned}
&M_L(c\bar{c}([^3S_1]_1) \to \psi(2S)) = 0.76\,\mathrm{GeV}^3 \\
&M_L(c\bar{c}([^3S_1]_8) \to \psi(2S)) \\
&M_L(c\bar{c}([^1S_0]_8) \to \psi(2S)) \\
&M_L(c\bar{c}([^3P_0]_8) \to \psi(2S))
\end{aligned} \tag{12}$$

3. Feed-down contribution from χ_{cJ}

$$\begin{aligned}
&M_L(c\bar{c}([^3P_0]_1) \to \chi_{c0}) = 0.054\,m_c^2\,\mathrm{GeV}^3 \\
&M_L(c\bar{c}([^3S_1]_8) \to \chi_{c0})
\end{aligned} \tag{13}$$

Hence for J/ψ we have to determine 10 parameters. Three color singlet matrix elements can be estimated from the wavefunctions of the heavy mesons. We use the following procedure to determine the remaining 7 color-octet components. CDF [23] has measured the feed-down contribution from the χ_{cJ} states to J/ψ production. We use this data to fit the octet matrix element $M_L(Q\bar{Q}([^3S_1]_8) \to \chi_{c0})$. Figure 1 shows different components of cross-section along with the CDF data

$$M_L(Q\bar{Q}([^3S_1]_8) \to \chi_{c0})/m^2_{\rm charm} = (0.00157 \pm 0.00159)\,{\rm GeV}^3\;, \tag{14}$$

where the error includes the change in the matrix elements when we change the lowest p_T included in the fit by 1 GeV. The $\chi^2/dof = 4.56$ is not very good because the (dominant) color-octet production is harder than the experimentally observed spectrum. We assume that the measured yields of prompt $\psi(2S)$ is not substantially contaminated by higher feed-downs and use combined fit of the following data sets

1. CMS results at $\sqrt{S} = 7$ TeV [8, 9]
2. ATLAS results at $\sqrt{S} = 7$ and 8 TeV [10]
3. CDF results at $\sqrt{S} = 1.96$ TeV [22]

to obtain color octet $\psi(2S)$ matrix elements. Figure 2 and Figure 3 shows the fitted values of color-singlet and color-octet cross-section components along with the measured $\psi(2S)$ cross-section. We found following values of $\psi(2S)$ color-octet matrix elements

$$\begin{aligned} M_L(c\bar{c}([^3S_1]_8) \to \psi(2S)) &= (0.00190 \pm 0.00002){\rm GeV}^3 \\ M_L(c\bar{c}([^1S_0]_8) \to \psi(2S)) &= (0.0264 \pm 0.0003){\rm GeV}^3 \\ &= M_L(c\bar{c}([^3P_0]_8) \to \psi(2S))/m^2_{\rm charm}\;, \end{aligned} \tag{15}$$

with a $\chi^2/dof = 00$. To fit the remaining 3 parameters we use the combined fit for the following results for J/ψ (direct+feed-down) yields

1. CMS results at $\sqrt{S} = 7$ TeV [8, 9]
2. ATLAS results at $\sqrt{S} = 7$ and 8 TeV [10]
3. CDF results at $\sqrt{S} = 1.96$ TeV [22]

Figure 4 and Figure 5 shows the fitted values of color-singlet and color-octet cross-section components along with the measured J/ψ cross-section. Using simultaneous fitting of these data-sets We obtain,

$$\begin{aligned} M_L(c\bar{c}([^3S_1]_8) \to J/\psi) &= (0.00317 \pm 0.00007){\rm GeV}^3 \\ M_L(c\bar{c}([^1S_0]_8) \to J/\psi) &= (0.0630 \pm 0.0015){\rm GeV}^3 \\ &= M_L(c\bar{c}([^3P_0]_8) \to J/\psi)/m^2_{\rm charm}\;, \end{aligned} \tag{16}$$

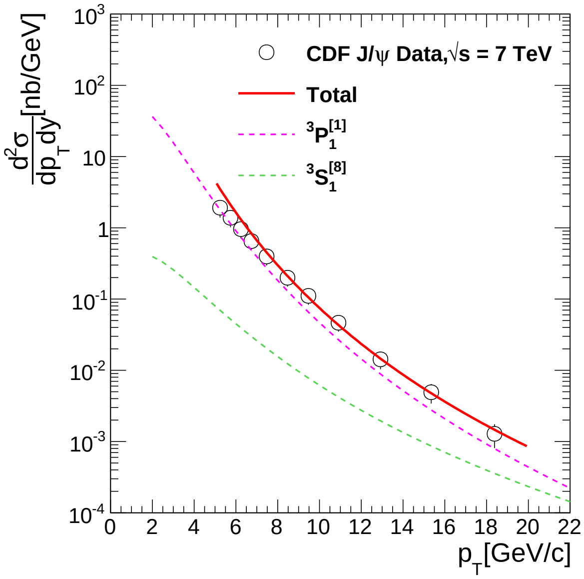

FIG. 1. (Color online) Differential production cross-section of J/ψ from χ_{c1} and χ_{c2} decay as a function of p_T measured by CDF experiment at $\sqrt{s} = 1.8$ TeV [23]. We use these data sets to constrain color octet LDMEs. Figure also shows our calculations for various components of χ_c croos-section.

with a $\chi^2/dof = 0$. For a more sophisticated fitting of the color-octet matrix elements including NLO effects, see [19–21].

III. RESULT AND DISCUSSION

Figure 6 (a) shows the differential production cross-section of prompt J/ψ as a function of transeverse momentum (p_T) compared with the CMS measurements [9]. We have calculated differential production cross-sections for all the relevant resonances. These cross sections are then appropriately scaled with proper branching fractions and total cross section for prompt J/ψ is calculated and shown in Fig. 6 (a). The ψ(2S) has largest contribution at high p_T while at low p_T contribution from χ_{c1} and χ_{c2} exceed the ψ(2S) contribution. After adding all the contributions, the p_T dependence of prompt J/ψ differential production cross-section are described reasonably well by our calculations. The $\psi(2S)$ has no significant feed-down contributions from higher mass states. We call this direct contribution as "prompt ψ(2S)" to be consistent with the J/ψ calculations. Figure 6(b) shows the differential production cross-section of prompt ψ(2S) as a function of p_T compared with the CMS measurements [9].

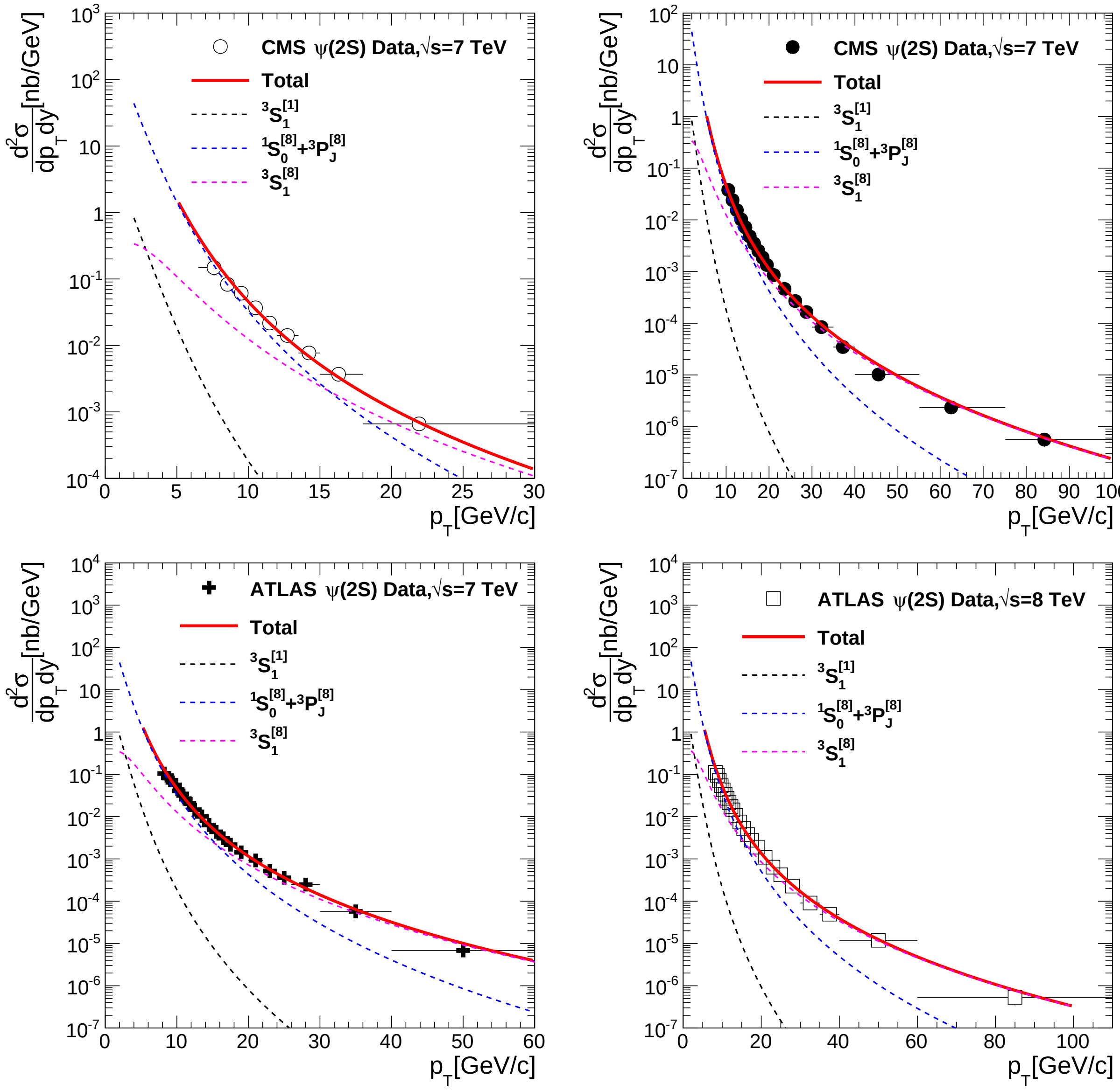

FIG. 2. (Color online) Differential production cross-section of ψ(2S) as a function of p_T collected by LHC experiments at $\sqrt{s}$ = 7 and 8 TeV [8–10]. We use these data sets to constrain color octet LDMEs. Figures also shows our calculations for various components of ψ(2S) croos-section.

Here also our calculations qualitatively reproduced the mesaured cross section.

Discription for old figures, should put new figures of cross section prediction at 14 TeV and describe the fitting figures.

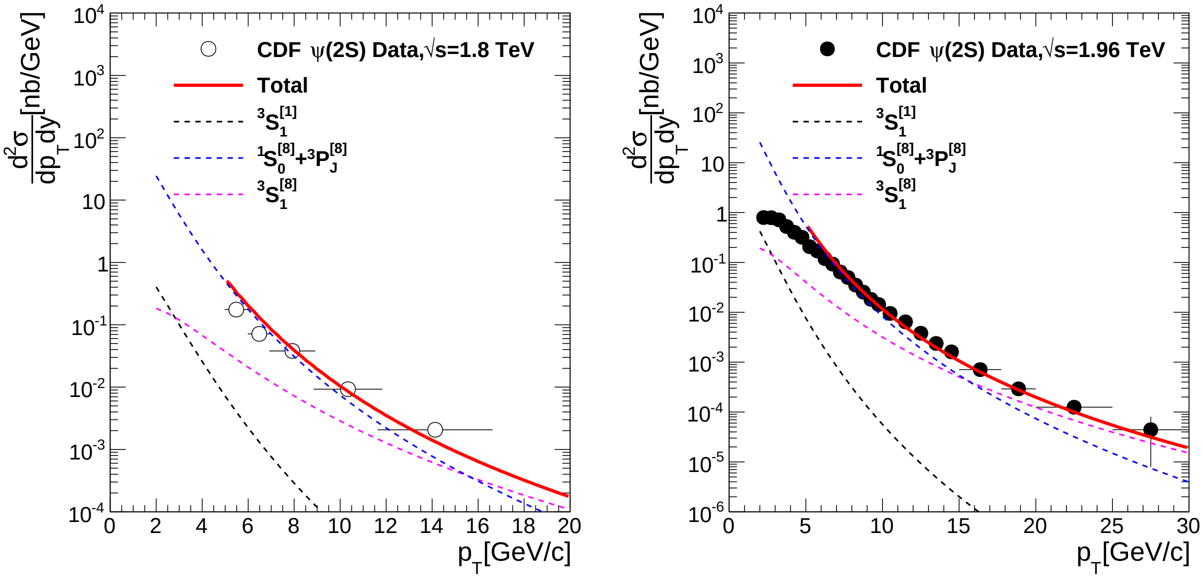

FIG. 3. (Color online) Differential production cross-section of ψ(2S) as a function of p_T collected by CDF experiment at $\sqrt{s} = 1.8$ TeV and $\sqrt{s} = 1.96$ TeV [22]. We use these data sets to constrain color octet LDMEs. Figures also shows our calculations for various components of ψ(2S) croos-section.

IV. SUMMARY

We have calculated the differential production cross-section of prompt J/ψ and prompt ψ(2S) as a function of transverse momentum. For the J/ψ meson all the relevent contributions from higher mass states are estimated. The ψ(2S) meson does not have significant contributions from higher mass states. The calculations for prompt J/ψ and prompt ψ(2S) are compared with the measured data at LHC. A fairly good agreement between measured data and calculations is observed in low p_T range. The reevaluation of LDME is in progress using latest data from LHC to achieve good description of data in the whole p_T range.

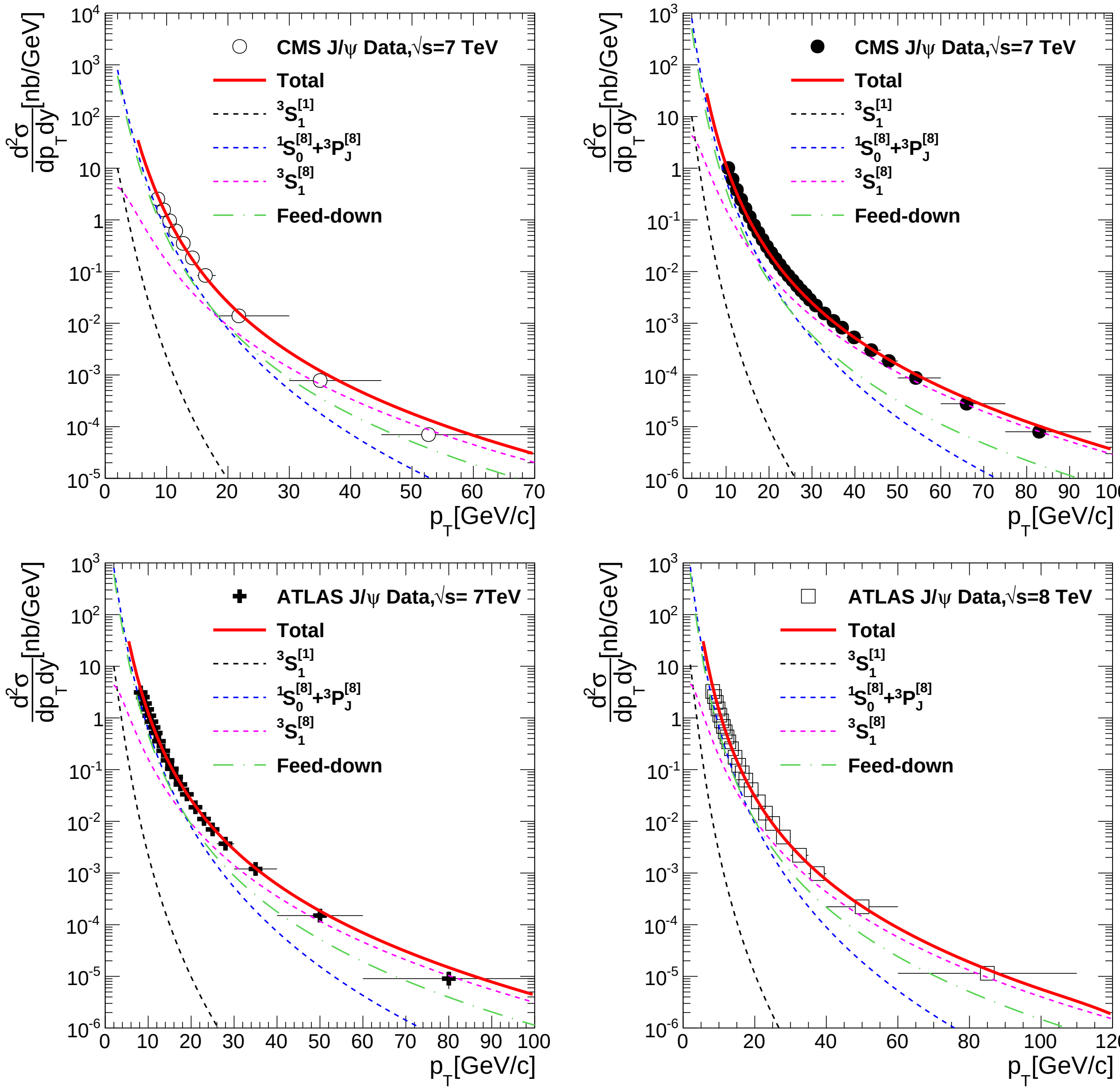

FIG. 4. (Color online) Differential production cross-section of J/ψ as a function of p_T collected by LHC experiments at $\sqrt{s} = 7$ and 8 TeV [8–10]. We use these data sets to constrain color octet LDMEs. Figures also shows our calculations for various components of J/ψ croos-section and feed-down contribution from higher charmonia states.

Appendix A: Short distance pQCD cross sections for quarkonia production

Here we list the lowest order QCD cross sections for the resonance production used in our calculations. We write the formulas in terms of the invariants $\hat{s}$,$\hat{t}$,$\hat{u}$. where $\hat{s}^2 + \hat{t}^2 + \hat{u}^2 = M^2$ and M is the mass of the resonance considered. The subprocesses of resonance production

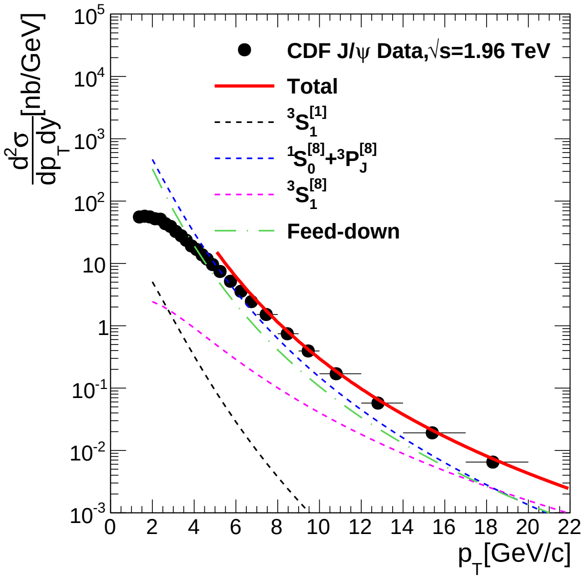

FIG. 5. (Color online) Differential production cross-section of J/ψ as a function of p_T collected by CDF experiment at $\sqrt{s} = 1.96$ TeV [22]. We use these data sets to constrain color octet LDMEs. Figures also shows our calculations for various components of J/ψ croos-section and feed-down contribution from higher charmonia states.

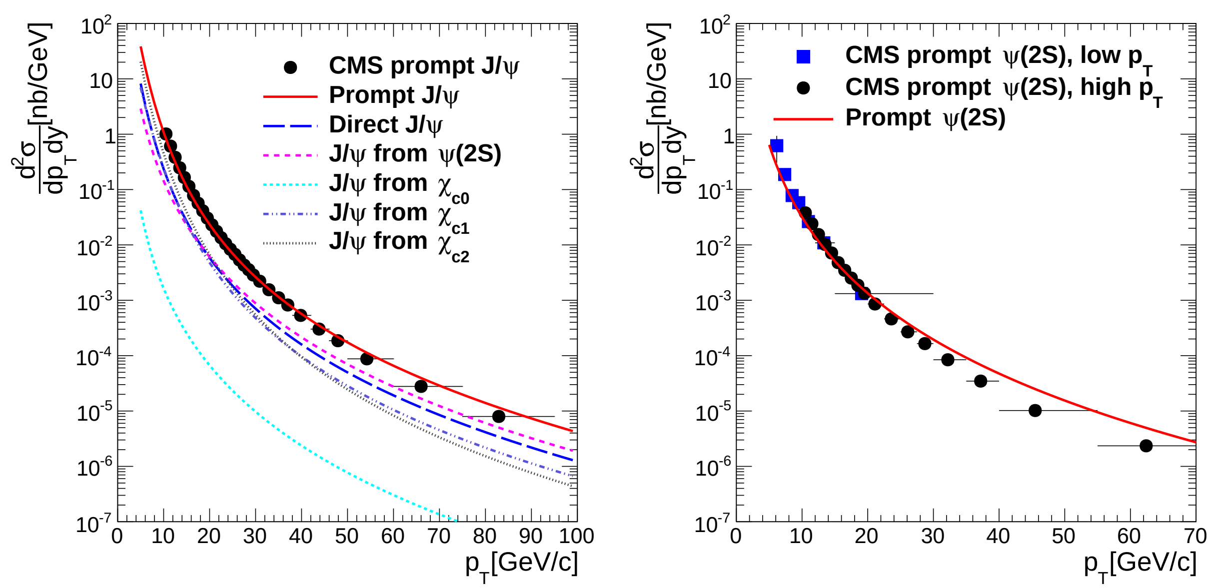

FIG. 6. (Color online) Differential production cross-section of J/ψ and $\psi(2S)$ as a function of p_T compared with the CMS [8, 9] data.

can be grouped as follows. To order α_s^2 one only has the gluon fusion processes, g g $\rightarrow^{(2S+1)}$ L_J. This process gives resonance with very small p_T, so we do not use these cross-sections in our calculations.

To order α_s^3, on the other hand, one has typically two-by-two scattering processes. The relevant cross sections are given below:

a. Color Singlet PQCD cross sections

- g q $\rightarrow$ $^{(2\mathrm{S}+1)}\mathrm{L_J}$ q or (q$\rightarrow$ $\bar{\mathrm{q}}$)

$$\begin{aligned}
\frac{d\sigma}{d\hat{t}}(^1S_0) =& \frac{2\pi{\alpha_s}^3(R_0)^2}{9M\hat{s}^2}\cdot\frac{(\hat{t}-M^2)^2-2\hat{s}\hat{u}}{(-\hat{t})(\hat{t}-M^2)^2}\\
\frac{d\sigma}{d\hat{t}}(^3P_0) =& \frac{8\pi{\alpha_s}^3(R_1')^2}{9M^3\hat{s}^2}\cdot\frac{(\hat{t}-3M^2)^2(\hat{s}^2+\hat{u}^2)}{(-\hat{t})(\hat{t}-M^2)^4}\\
\frac{d\sigma}{d\hat{t}}(^3P_1) =& \frac{16\pi{\alpha_s}^3(R_1')^2}{3M^3\hat{s}^2}\cdot\frac{-\hat{t}(\hat{s}^2+\hat{u}^2)-4M^2\hat{s}\hat{u}}{(\hat{t}-M^2)^4}\\
\frac{d\sigma}{d\hat{t}}(^3P_2) =& \frac{16\pi{\alpha_s}^3(R_1')^2}{9M^3\hat{s}^2}\cdot\\
& \frac{(\hat{t}-M^2)^2(\hat{t}^2+6M^4)-2\hat{s}\hat{u}(\hat{t}^2-6M^2(\hat{t}-M^2))}{(-\hat{t})(\hat{t}-M^2)^4}
\end{aligned} \tag{A1}$$

- q $\bar{\mathrm{q}}$ $\rightarrow$ $^{(2\mathrm{S}+1)}\mathrm{L_J}$ g

$$\frac{d\sigma}{d\hat{t}}(^{(2\mathrm{S}+1)}\mathrm{L_J}) = -\frac{8}{3}\frac{\hat{t}^2}{\hat{s}^2}\frac{d\sigma}{d\hat{t}}(\mathrm{gq}\rightarrow^{(2\mathrm{S}+1)}\mathrm{L_J q})|_{\hat{t}\leftrightarrow\hat{u}} \tag{A2}$$

- g g $\rightarrow$ $^{(2\mathrm{S}+1)}\mathrm{L_J}$ g

$$\begin{aligned}
\frac{d\sigma}{d\hat{t}}(^3S_1) =& \frac{5\pi{\alpha_s}^3(R_0)^2}{9M\hat{s}^2}\cdot\frac{M^2}{(\hat{s}-M^2)^2(\hat{t}-M^2)^2(\hat{u}-M^2)^2}\\
& \cdot\{[\hat{s}^2(\hat{s}-M^2)^2]+[\hat{s}\rightarrow\hat{t}]+[\hat{s}\rightarrow\hat{u}]\}\\
\frac{d\sigma}{d\hat{t}}(^1S_0) =& \frac{\pi{\alpha_s}^3(R_0)^2}{2M\hat{s}^2}\frac{1}{\hat{s}\hat{t}\hat{u}(\hat{s}-M^2)^2(\hat{t}-M^2)^2(\hat{u}-M^2)^2}\\
& \cdot\{[\hat{s}^4(\hat{s}-M^2)^2((\hat{s}-M^2)^2+2M^4)\\
& -\frac{4}{3}\hat{s}\hat{t}\hat{u}(\hat{s}^2+\hat{t}^2+\hat{u}^2)(\hat{s}-M^2)(\hat{t}-M^2)(\hat{u}-M^2)\\
& +\frac{16}{3}M^2\hat{s}\hat{t}\hat{u}(\hat{s}^2\hat{t}^2+\hat{s}^2\hat{u}^2+\hat{t}^2\hat{u}^2)\\
& +\frac{28}{3}M^4\hat{s}^2\hat{t}^2\hat{u}^2]+[\hat{s}\leftrightarrow\hat{t}]+[\hat{s}\leftrightarrow\hat{u}]\}
\end{aligned} \tag{A3}$$

We define two new variables as a combination of $\hat{s}$, $\hat{t}$ and $\hat{u}$ which can be used to define the g g $\rightarrow$ $^{(2S+1)}\mathrm{L_J}$ g cross sections.

$$\begin{aligned} P &= \hat{s}\hat{t} + \hat{t}\hat{u} + \hat{u}\hat{s} \\ Q &= \hat{s}\hat{t}\hat{u} \end{aligned} \tag{A4}$$

$$\begin{aligned}
\frac{d\sigma}{d\hat{t}}(^1S_0) = & \ \frac{\pi{\alpha_s}^3(R_0)^2}{M\hat{s}^2}\frac{P^2(M^8-2M^4P+P^2+2M^2Q)}{Q(Q-M^2P)^2} \\
\frac{d\sigma}{d\hat{t}}(^3S_1) = & \ \frac{10\pi{\alpha_s}^3(R_0)^2}{9\hat{s}^2}\frac{M(P^2-M^2Q)}{(Q-M^2P)^2} \\
\frac{d\sigma}{d\hat{t}}(^1P_1) = & \ \frac{40\pi{\alpha_s}^3(R_1')^2}{3M\hat{s}^2}\frac{[-M^{10}P+M^6P^2+Q(5M^8-7M^4P+2P^2)+4M^2Q^2]}{(Q-M^2P)^3} \\
\frac{d\sigma}{d\hat{t}}(^3P_0) = & \ \frac{4\pi{\alpha_s}^3(R_1')^2}{M^3\hat{s}^2}\frac{1}{Q(Q-M^2P)^4}[9M^4P^4(M^8-2M^4P+P^2) \\
& -6M^2P^3Q(2M^8-5M^4P+P^2) \\
& -P^2Q^2(M^8+2M^4P-P^2) \\
& +2M^2PQ^3(M^4-P)+6M^4Q^4] \\
\frac{d\sigma}{d\hat{t}}(^3P_1) = & \ \frac{12\pi{\alpha_s}^3(R_1')^2}{M^3\hat{s}^2}\frac{P^2\{M^2P^2(M^4-4P)-2Q(M^8-5M^4P-P^2)-15M^2Q^2\}}{(Q-M^2P)^4} \\
\frac{d\sigma}{d\hat{t}}(^3P_2) = & \ \frac{4\pi{\alpha_s}^3(R_1')^2}{M^3\hat{s}^2}\frac{1}{Q(Q-M^2P)^4} \\
& \{12M^4P^4(M^8-2M^4P+P^2)-3M^2P^3Q(8M^8-M^4P+4P^2) \\
& -2P^2Q^2(7M^8-43M^4P-P^2)+M^2PQ^3(16M^4-61P) \\
& +12M^4Q^4\}
\end{aligned} \tag{A5}$$

b. **Color Octet PQCD cross sections**

We list below short distance squared amplitudes for $2 \rightarrow 2$ scattering processes which mediate color-octet quarkonia production. These expressions are averaged over initial spins and colors of the two incident partons. The helicity levels of outgoing $J=1$ and $J=2$ pairs are labeled by the subscript h.

- q $\bar{\text{q}}$ $\to Q\bar{Q}[^{(2\mathrm{S}+1)}\mathrm{L}_{\mathrm{J}}^{(8)}]$ g

$$
\begin{aligned}
\bar{\sum} |\mathcal{A}(q\bar{q} \to Q\overline{Q}[^1S_0^{(8)}]g)|^2 &= \frac{5(4\pi\alpha_s)^3}{27M}\frac{\hat{t}^2+\hat{u}^2}{\hat{s}(\hat{s}-M^2)^2} \\
\bar{\sum_{h=0}} |\mathcal{A}(q\bar{q} \to Q\overline{Q}[^3S_1^{(8)}]g)|^2 &= \frac{8(4\pi\alpha_s)^3}{81M^3}\frac{M^2\hat{\mathrm{s}}}{(\hat{\mathrm{s}}-M^2)^4}\left[4(\hat{\mathrm{t}}^2+\hat{\mathrm{u}}^2)-\hat{\mathrm{t}}\hat{\mathrm{u}}\right] \\
\bar{\sum_{|h|=1}} |\mathcal{A}(q\bar{q} \to Q\overline{Q}[^3S_1^{(8)}]g)|^2 &= \frac{2(4\pi\alpha_s)^3}{81M^3}\frac{\hat{\mathrm{s}}^2+M^4}{(\hat{\mathrm{s}}-M^2)^4}\frac{\hat{\mathrm{t}}^2+\hat{\mathrm{u}}^2}{\hat{\mathrm{t}}\hat{\mathrm{u}}}\left[4(\hat{\mathrm{t}}^2+\hat{\mathrm{u}}^2)-\hat{\mathrm{t}}\hat{\mathrm{u}}\right] \\
\bar{\sum} |\mathcal{A}(q\bar{q} \to Q\overline{Q}[^3P_0^{(8)}]g)|^2 &= \frac{20(4\pi\alpha_s)^3}{81M^3}\frac{(\hat{\mathrm{s}}-3M^2)^2(\hat{\mathrm{t}}^2+\hat{\mathrm{u}}^2)}{\hat{\mathrm{s}}(\hat{\mathrm{s}}-M^2)^4} \\
\bar{\sum_{h=0}} |\mathcal{A}(q\bar{q} \to Q\overline{Q}[^3P_1^{(8)}]g)|^2 &= \frac{40(4\pi\alpha_s)^3}{81M^3}\frac{\hat{\mathrm{s}}(\hat{\mathrm{t}}^2+\hat{\mathrm{u}}^2)}{(\hat{\mathrm{s}}-M^2)^4} \\
\bar{\sum_{|h|=1}} |\mathcal{A}(q\bar{q} \to Q\overline{Q}[^3P_1^{(8)}]g)|^2 &= \frac{160(4\pi\alpha_s)^3}{81M^3}\frac{M^2\hat{\mathrm{t}}\hat{\mathrm{u}}}{(\hat{\mathrm{s}}-M^2)^4} \\
\bar{\sum_{h=0}} |\mathcal{A}(q\bar{q} \to Q\overline{Q}[^3P_2^{(8)}]g)|^2 &= \frac{8(4\pi\alpha_s)^3}{81M^3}\frac{\hat{\mathrm{s}}(\hat{\mathrm{t}}^2+\hat{\mathrm{u}}^2)}{(\hat{\mathrm{s}}-M^2)^4} \\
\bar{\sum_{|h|=1}} |\mathcal{A}(q\bar{q} \to Q\overline{Q}[^3P_2^{(8)}]g)|^2 &= \frac{32(4\pi\alpha_s)^3}{27M^3}\frac{M^2\hat{\mathrm{t}}\hat{\mathrm{u}}}{(\hat{\mathrm{s}}-M^2)^4} \\
\bar{\sum_{|h|=2}} |\mathcal{A}(q\bar{q} \to Q\overline{Q}[^3P_2^{(8)}]g)|^2 &= \frac{16(4\pi\alpha_s)^3}{27M^3}\frac{M^4(\hat{\mathrm{t}}^2+\hat{\mathrm{u}}^2)}{\hat{\mathrm{s}}(\hat{\mathrm{s}}-M^2)^4}
\end{aligned}
\tag{A6}
$$

- g q $\to Q\bar{Q}[^{(2S+1)}L_J^{(8)}]$ q

$$
\begin{aligned}
\bar{\sum}|\mathcal{A}(gq\to Q\overline{Q}[^1S_0^{(8)}]q)|^2 &= -\frac{5(4\pi\alpha_s)^3}{72M}\frac{\hat{s}^2+\hat{u}^2}{\hat{t}(\hat{t}-M^2)^2}\\
\bar{\sum_{h=0}}|\mathcal{A}(gq\to Q\overline{Q}[^3S_1^{(8)}]q)|^2 &= -\frac{(4\pi\alpha_s)^3}{54M^3}\frac{M^2\hat{t}\big[4(\hat{s}^2+\hat{u}^2)-\hat{s}\hat{u}\big]}{\big[(\hat{s}-M^2)(\hat{t}-M^2)\big]^2}\\
\bar{\sum_{|h|=1}}|\mathcal{A}(gq\to Q\overline{Q}[^3S_1^{(8)}]q)|^2 &= -\frac{(4\pi\alpha_s)^3}{108M^3}\\
&\times\frac{(\hat{s}^2+\hat{u}^2+2M^2\hat{t})(\hat{s}-M^2)^2-2M^2\hat{s}\hat{t}\hat{u}}{\hat{s}\hat{u}\big[(\hat{s}-M^2)(\hat{t}-M^2)\big]^2}\\
&\times\big[4(\hat{s}^2+\hat{u}^2)-\hat{s}\hat{u}\big]\\
\bar{\sum}|\mathcal{A}(gq\to Q\overline{Q}[^3P_0^{(8)}]q)|^2 &= -\frac{5(4\pi\alpha_s)^3}{54M^3}\frac{(\hat{t}-3M^2)^2(\hat{s}^2+\hat{u}^2)}{\hat{t}(\hat{t}-M^2)^4}\\
\bar{\sum_{h=0}}|\mathcal{A}(gq\to Q\overline{Q}[^3P_1^{(8)}]q)|^2 &= -\frac{5(4\pi\alpha_s)^3}{27M^3}\frac{\hat{t}\big[\hat{s}^2(\hat{s}-M^2)^2+\hat{u}^2(\hat{s}+M^2)^2\big]}{(\hat{t}-M^2)^4(\hat{s}-M^2)^2}\\
\bar{\sum_{|h|=1}}|\mathcal{A}(gq\to Q\overline{Q}[^3P_1^{(8)}]q)|^2 &= -\frac{20(4\pi\alpha_s)^3}{27M^3}\frac{M^2\hat{s}\hat{u}(\hat{t}^2+\hat{t}\hat{u}+\hat{u}^2)}{(\hat{t}-M^2)^4(\hat{s}-M^2)^2}\\
\bar{\sum_{h=0}}|\mathcal{A}(gq\to Q\overline{Q}[^3P_2^{(8)}]q)|^2 &= -\frac{(4\pi\alpha_s)^3}{27M^3}\frac{\hat{t}}{(\hat{t}-M^2)^4}\\
&\times\big[\hat{s}^2+\hat{u}^2+12M^2\hat{s}\hat{u}^2\frac{\hat{s}^2+M^2\hat{s}+M^4}{(\hat{s}-M^2)^4}\big]\\
\bar{\sum_{|h|=1}}|\mathcal{A}(gq\to Q\overline{Q}[^3P_2^{(8)}]q)|^2 &= -\frac{4(4\pi\alpha_s)^3}{9M^3}\frac{M^2\hat{s}\hat{u}}{(\hat{t}-M^2)^4}\\
&\times\frac{(\hat{s}-M^2)^2(\hat{s}^2+M^4)-(\hat{s}+M^2)^2\hat{t}\hat{u}}{(\hat{s}-M^2)^4}\\
\bar{\sum_{|h|=2}}|\mathcal{A}(gq\to Q\overline{Q}[^3P_2^{(8)}]q)|^2 &= -\frac{2(4\pi\alpha_s)^3}{9M^3}\frac{M^4}{\hat{t}(\hat{t}-M^2)^4}\\
&\times\big[\hat{s}^2+\hat{u}^2+2\hat{s}^2\hat{t}\hat{u}\frac{(\hat{s}-M^2)(2\hat{t}+\hat{u})-\hat{u}^2}{(\hat{s}-M^2)^4}\big]
\end{aligned}
\tag{A7}
$$

- g g $\to Q\bar{Q}[^{(2S+1)}L_J^{(8)}]$ g (The $gg\to Q\overline{Q}[^3P_J^{(8)}]\ g$ squared amplitudes are expressed in terms of the variables ŝ and $\hat{z} \equiv \sqrt{\hat{t}\hat{u}}$.)

$$
\begin{aligned}
\overline{\sum} |\mathcal{A}(gg \to Q\overline{Q}[^1S_0^{(8)}]g)|^2 &= \frac{5(4\pi\alpha_s)^3}{16M}\left[\hat{s}^2(\hat{s}-M^2)^2 + \hat{s}\hat{t}\hat{u}(M^2-2\hat{s}) + (\hat{t}\hat{u})^2\right] \\
&\times \frac{(\hat{s}^2 - M^2\hat{s} + M^4)^2 - \hat{t}\hat{u}(2\hat{t}^2 + 3\hat{t}\hat{u} + 2\hat{u}^2)}{\hat{s}\hat{t}\hat{u}\left[(\hat{s}-M^2)(\hat{t}-M^2)(\hat{u}-M^2)\right]^2} \\
\overline{\sum_{h=0}} |\mathcal{A}(gg \to Q\overline{Q}[^3S_1^{(8)}]g)|^2 &= -\frac{(4\pi\alpha_s)^3}{144M^3}\frac{2M^2\hat{s}}{(\hat{s}-M^2)^2}(\hat{t}^2+\hat{u}^2)\hat{t}\hat{u} \\
&\times \frac{27(\hat{s}\hat{t}+\hat{t}\hat{u}+\hat{u}\hat{s}) - 19M^4}{\left[(\hat{s}-M^2)(\hat{t}-M^2)(\hat{u}-M^2)\right]^2} \\
\overline{\sum_{|h|=1}} |\mathcal{A}(gg \to Q\overline{Q}[^3S_1^{(8)}]g)|^2 &= -\frac{(4\pi\alpha_s)^3}{144M^3}\frac{\hat{s}^2}{(\hat{s}-M^2)^2} \\
&\times \left[(\hat{s}-M^2)^4 + \hat{t}^4 + \hat{u}^4 + 2M^4\left(\frac{\hat{t}\hat{u}}{\hat{s}}\right)^2\right] \\
&\times \frac{27(\hat{s}\hat{t}+\hat{t}\hat{u}+\hat{u}\hat{s}) - 19M^4}{\left[(\hat{s}-M^2)(\hat{t}-M^2)(\hat{u}-M^2)\right]^2} \\
\overline{\sum} |\mathcal{A}(gg \to Q\overline{Q}[^3P_0^{(8)}]g)|^2 &= \frac{5(4\pi\alpha_s)^3}{12M^3}\frac{1}{\left[\hat{s}\hat{z}^2(\hat{s}-M^2)^4(\hat{s}M^2+\hat{z}^2)^4\right]} \\
&\times \Big\{\hat{s}^2\hat{z}^4(\hat{s}^2-\hat{z}^2)^4 + M^2\hat{s}\hat{z}^2(\hat{s}^2-\hat{z}^2)^2(3\hat{s}^2-2\hat{z}^2)(2\hat{s}^4-6\hat{s}^2\hat{z}^2+3\hat{z}^4) \\
&+ M^4\left[9\hat{s}^{12} - 84\hat{s}^{10}\hat{z}^2 + 265\hat{s}^8\hat{z}^4 - 382\hat{s}^6\hat{z}^6 + 276\hat{s}^4\hat{z}^8 - 88\hat{s}^2\hat{z}^{10} + 9\hat{z}^{12}\right] \\
&- M^6\hat{s}\left[54\hat{s}^{10} - 357\hat{s}^8\hat{z}^2 + 844\hat{s}^6\hat{z}^4 - 898\hat{s}^4\hat{z}^6 + 439\hat{s}^2\hat{z}^8 - 81\hat{z}^{10}\right] \\
&+ M^8\left[153\hat{s}^{10} - 798\hat{s}^8\hat{z}^2 + 1415\hat{s}^6\hat{z}^4 - 1041\hat{s}^4\hat{z}^6 + 301\hat{s}^2\hat{z}^8 - 18\hat{z}^{10}\right] \\
&- M^{10}\hat{s}\left[270\hat{s}^8 - 1089\hat{s}^6\hat{z}^2 + 1365\hat{s}^4\hat{z}^4 - 616\hat{s}^2\hat{z}^6 + 87\hat{z}^8\right] \\
&+ M^{12}\left[324\hat{s}^8 - 951\hat{s}^6\hat{z}^2 + 769\hat{s}^4\hat{z}^4 - 189\hat{s}^2\hat{z}^6 + 9\hat{z}^8\right] \\
&- 9M^{14}\hat{s}\left[(6\hat{s}^2-\hat{z}^2)(5\hat{s}^4 - 9\hat{s}^2\hat{z}^2 + 3\hat{z}^4)\right] \\
&+ 3M^{16}\hat{s}^2\left[51\hat{s}^4 - 59\hat{s}^2\hat{z}^2 + 12\hat{z}^4\right] \\
&- 27M^{18}\hat{s}^3\left[2\hat{s}^2 - \hat{z}^2\right] \\
&+ 9M^{20}\hat{s}^4\Big\}
\end{aligned}
\tag{A8}
$$

$$
\begin{aligned}
\sum_{h=0}^{-}|\mathcal{A}(gg\to Q\overline{Q}[^3P_1^{(8)}]g)|^2 &= \frac{5(4\pi\alpha_s)^3}{6M^3}\frac{1}{\big[(\hat{\mathrm{s}}-M^2)^4(\hat{\mathrm{s}}M^2+\hat{\mathrm{z}}^2)^4\big]} \\
&\times \hat{\mathrm{s}}\hat{\mathrm{z}}^2\big[(\hat{\mathrm{s}}^2-\hat{\mathrm{z}}^2)^2-2M^2\hat{\mathrm{s}}\hat{\mathrm{z}}^2-M^4(\hat{\mathrm{s}}^2+2\hat{\mathrm{z}}^2)+M^8\big] \\
&\times \big[(\hat{\mathrm{s}}^2-\hat{\mathrm{z}}^2)^2-M^2\hat{\mathrm{s}}(2\hat{\mathrm{s}}^2-\hat{\mathrm{z}}^2)+M^4\hat{\mathrm{s}}^2\big] \\
\sum_{|h|=1}^{-}|\mathcal{A}(gg\to Q\overline{Q}[^3P_1^{(8)}]g)|^2 &= \frac{5(4\pi\alpha_s)^3}{6M^3}\frac{1}{\big[(\hat{\mathrm{s}}-M^2)^4(\hat{\mathrm{s}}M^2+\hat{\mathrm{z}}^2)^4\big]} \\
&\times M^2\Big\{2(\hat{\mathrm{s}}^2-\hat{\mathrm{z}}^2)^2(\hat{\mathrm{s}}^6-4\hat{\mathrm{s}}^4\hat{\mathrm{z}}^2+\hat{\mathrm{s}}^2\hat{\mathrm{z}}^4-\hat{\mathrm{z}}^6) \\
&- M^2\hat{\mathrm{s}}(2\hat{\mathrm{s}}^2-\hat{\mathrm{z}}^2)(5\hat{\mathrm{s}}^6-17\hat{\mathrm{s}}^4\hat{\mathrm{z}}^2+9\hat{\mathrm{s}}^2\hat{\mathrm{z}}^4-\hat{\mathrm{z}}^6) \\
&+ M^4(21\hat{\mathrm{s}}^8-49\hat{\mathrm{s}}^6\hat{\mathrm{z}}^2+21\hat{\mathrm{s}}^4\hat{\mathrm{z}}^4-4\hat{\mathrm{s}}^2\hat{\mathrm{z}}^6+\hat{\mathrm{z}}^8) \\
&- M^6\hat{\mathrm{s}}(24\hat{\mathrm{s}}^6-30\hat{\mathrm{s}}^4\hat{\mathrm{z}}^2+6\hat{\mathrm{s}}^2\hat{\mathrm{z}}^4-\hat{\mathrm{z}}^6) \\
&+ M^8\hat{\mathrm{s}}^2(16\hat{\mathrm{s}}^4-9\hat{\mathrm{s}}^2\hat{\mathrm{z}}^2+2\hat{\mathrm{z}}^4) \\
&- M^{10}\hat{\mathrm{s}}^3(6\hat{\mathrm{s}}^2-\hat{\mathrm{z}}^2) \\
&+ M^{12}\hat{\mathrm{s}}^4\Big\} \\
\sum_{h=0}^{-}|\mathcal{A}(gg\to Q\overline{Q}[^3P_2^{(8)}]g)|^2 &= \frac{(4\pi\alpha_s)^3}{6M^3}\frac{\hat{\mathrm{s}}\hat{\mathrm{z}}^2}{\big[(\hat{\mathrm{s}}-M^2)^6(\hat{\mathrm{s}}M^2+\hat{\mathrm{z}}^2)^4\big]} \\
&\Big\{\hat{\mathrm{s}}^2(\hat{\mathrm{s}}^2-\hat{\mathrm{z}}^2)^4-M^2\hat{\mathrm{s}}\hat{\mathrm{z}}^2(\hat{\mathrm{s}}^2-\hat{\mathrm{z}}^2)^2(11\hat{\mathrm{s}}^2+2\hat{\mathrm{z}}^2) \\
&+ M^4\big[\hat{\mathrm{s}}^8-12\hat{\mathrm{s}}^6\hat{\mathrm{z}}^2+41\hat{\mathrm{s}}^4\hat{\mathrm{z}}^4-20\hat{\mathrm{s}}^2\hat{\mathrm{z}}^6+\hat{\mathrm{z}}^8\big] \\
&- M^6\hat{\mathrm{s}}\big[4\hat{\mathrm{s}}^6-26\hat{\mathrm{s}}^4\hat{\mathrm{z}}^2-\hat{\mathrm{s}}^2\hat{\mathrm{z}}^4-5\hat{\mathrm{z}}^6\big] \\
&+ M^8\big[29\hat{\mathrm{s}}^6-114\hat{\mathrm{s}}^4\hat{\mathrm{z}}^2+108\hat{\mathrm{s}}^2\hat{\mathrm{z}}^4-10\hat{\mathrm{z}}^6\big] \\
&- M^{10}\hat{\mathrm{s}}\big[65\hat{\mathrm{s}}^4-104\hat{\mathrm{s}}^2\hat{\mathrm{z}}^2-33\hat{\mathrm{z}}^4\big] \\
&+ M^{12}\big[54\hat{\mathrm{s}}^4-20\hat{\mathrm{s}}^2\hat{\mathrm{z}}^2+7\hat{\mathrm{z}}^4\big] \\
&- M^{14}\hat{\mathrm{s}}\big[23\hat{\mathrm{s}}^2+5\hat{\mathrm{z}}^2\big] \\
&+ 7M^{16}\hat{\mathrm{s}}^2\Big\}
\end{aligned}
\tag{A9}
$$

$$\sum_{|h|=1}^{-} |\mathcal{A}(gg \to Q\overline{Q}[^3P_2^{(8)}]g)|^2 = \frac{(4\pi\alpha_s)^3}{2M^3}\frac{M^2}{\left[(\hat{\mathrm{s}}-M^2)^6(\hat{\mathrm{s}}M^2+\hat{\mathrm{z}}^2)^4\right]}$$

$$\times\Big\{2\hat{\mathrm{s}}^2(\hat{\mathrm{s}}^2-\hat{\mathrm{z}}^2)^2(\hat{\mathrm{s}}^6-4\hat{\mathrm{s}}^4\hat{\mathrm{z}}^2+\hat{\mathrm{s}}^2\hat{\mathrm{z}}^4-\hat{\mathrm{z}}^6)$$

$$-M^2\hat{\mathrm{s}}\big[10\hat{\mathrm{s}}^{10}-37\hat{\mathrm{s}}^8\hat{\mathrm{z}}^2+19\hat{\mathrm{s}}^6\hat{\mathrm{z}}^4+11\hat{\mathrm{s}}^4\hat{\mathrm{z}}^6-\hat{\mathrm{s}}^2\hat{\mathrm{z}}^8-4\hat{\mathrm{z}}^{10}\big]$$

$$+M^4\big[25\hat{\mathrm{s}}^{10}-61\hat{\mathrm{s}}^8\hat{\mathrm{z}}^2+27\hat{\mathrm{s}}^6\hat{\mathrm{z}}^4-34\hat{\mathrm{s}}^4\hat{\mathrm{z}}^6+23\hat{\mathrm{s}}^2\hat{\mathrm{z}}^8-2\hat{\mathrm{z}}^{10}\big]$$

$$-M^6\hat{\mathrm{s}}\big[42\hat{\mathrm{s}}^8-77\hat{\mathrm{s}}^6\hat{\mathrm{z}}^2+41\hat{\mathrm{s}}^4\hat{\mathrm{z}}^4-22\hat{\mathrm{s}}^2\hat{\mathrm{z}}^6+17\hat{\mathrm{z}}^8\big]$$

$$+M^8\big[53\hat{\mathrm{s}}^8-88\hat{\mathrm{s}}^6\hat{\mathrm{z}}^2+69\hat{\mathrm{s}}^4\hat{\mathrm{z}}^4-68\hat{\mathrm{s}}^2\hat{\mathrm{z}}^6+3\hat{\mathrm{z}}^8\big]$$

$$-M^{10}\hat{\mathrm{s}}\big[54\hat{\mathrm{s}}^6-85\hat{\mathrm{s}}^4\hat{\mathrm{z}}^2+60\hat{\mathrm{s}}^2\hat{\mathrm{z}}^4-9\hat{\mathrm{z}}^6\big]$$

$$+M^{12}\hat{\mathrm{s}}^2\big[43\hat{\mathrm{s}}^4-47\hat{\mathrm{s}}^2\hat{\mathrm{z}}^2+20\hat{\mathrm{z}}^4\big]$$

$$-M^{14}\hat{\mathrm{s}}^3\big[22\hat{\mathrm{s}}^2-9\hat{\mathrm{z}}^2\big]$$

$$+5M^{16}\hat{\mathrm{s}}^4\Big\}$$

$$\sum_{|h|=2}^{-} |\mathcal{A}(gg \to Q\overline{Q}[^3P_2^{(8)}]g)|^2 = \frac{(4\pi\alpha_s)^3}{2M^3}\frac{M^4}{\left[\hat{\mathrm{s}}\hat{\mathrm{z}}^2(\hat{\mathrm{s}}-M^2)^6(\hat{\mathrm{s}}M^2+\hat{\mathrm{z}}^2)^4\right]}$$

$$\times\Big\{2\hat{\mathrm{s}}^2\big[\hat{\mathrm{s}}^{12}-8\hat{\mathrm{s}}^{10}\hat{\mathrm{z}}^2+22\hat{\mathrm{s}}^8\hat{\mathrm{z}}^4-24\hat{\mathrm{s}}^6\hat{\mathrm{z}}^6+10\hat{\mathrm{s}}^4\hat{\mathrm{z}}^8-3\hat{\mathrm{s}}^2\hat{\mathrm{z}}^{10}+\hat{\mathrm{z}}^{12}\big]$$

$$-M^2\hat{\mathrm{s}}\big[16\hat{\mathrm{s}}^{12}-102\hat{\mathrm{s}}^{10}\hat{\mathrm{z}}^2+210\hat{\mathrm{s}}^8\hat{\mathrm{z}}^4-153\hat{\mathrm{s}}^6\hat{\mathrm{z}}^6+36\hat{\mathrm{s}}^4\hat{\mathrm{z}}^8-6\hat{\mathrm{s}}^2\hat{\mathrm{z}}^{10}+4\hat{\mathrm{z}}^{12}\big]$$

$$+M^4\big[60\hat{\mathrm{s}}^{12}-306\hat{\mathrm{s}}^{10}\hat{\mathrm{z}}^2+482\hat{\mathrm{s}}^8\hat{\mathrm{z}}^4-271\hat{\mathrm{s}}^6\hat{\mathrm{z}}^6+77\hat{\mathrm{s}}^4\hat{\mathrm{z}}^8-18\hat{\mathrm{s}}^2\hat{\mathrm{z}}^{10}+2\hat{\mathrm{z}}^{12}\big]$$

$$-M^6\hat{\mathrm{s}}\big[140\hat{\mathrm{s}}^{10}-573\hat{\mathrm{s}}^8\hat{\mathrm{z}}^2+710\hat{\mathrm{s}}^6\hat{\mathrm{z}}^4-344\hat{\mathrm{s}}^4\hat{\mathrm{z}}^6+91\hat{\mathrm{s}}^2\hat{\mathrm{z}}^8-18\hat{\mathrm{z}}^{10}\big]$$

$$+M^8\big[226\hat{\mathrm{s}}^{10}-741\hat{\mathrm{s}}^8\hat{\mathrm{z}}^2+737\hat{\mathrm{s}}^6\hat{\mathrm{z}}^4-310\hat{\mathrm{s}}^4\hat{\mathrm{z}}^6+77\hat{\mathrm{s}}^2\hat{\mathrm{z}}^8-4\hat{\mathrm{z}}^{10}\big]$$

$$-M^{10}\hat{\mathrm{s}}\big[264\hat{\mathrm{s}}^8-686\hat{\mathrm{s}}^6\hat{\mathrm{z}}^2+541\hat{\mathrm{s}}^4\hat{\mathrm{z}}^4-177\hat{\mathrm{s}}^2\hat{\mathrm{z}}^6+25\hat{\mathrm{z}}^8\big]$$

$$+M^{12}\big[226\hat{\mathrm{s}}^8-452\hat{\mathrm{s}}^6\hat{\mathrm{z}}^2+261\hat{\mathrm{s}}^4\hat{\mathrm{z}}^4-55\hat{\mathrm{s}}^2\hat{\mathrm{z}}^6+2\hat{\mathrm{z}}^8\big]$$

$$-M^{14}\hat{\mathrm{s}}\big[140\hat{\mathrm{s}}^6-201\hat{\mathrm{s}}^4\hat{\mathrm{z}}^2+71\hat{\mathrm{s}}^2\hat{\mathrm{z}}^4-6\hat{\mathrm{z}}^6\big]$$

$$+M^{16}\hat{\mathrm{s}}^2\big[60\hat{\mathrm{s}}^4-53\hat{\mathrm{s}}^2\hat{\mathrm{z}}^2+8\hat{\mathrm{z}}^4\big]$$

$$-2M^{18}\hat{\mathrm{s}}^3\big[8\hat{\mathrm{s}}^2-3\hat{\mathrm{z}}^2\big]$$

$$+2M^{20}\hat{\mathrm{s}}^4\Big\}$$

(A10)

[1] T. Matsui and H. Satz, "J/ψ Suppression by Quark-Gluon Plasma Formation", Phys. Lett. B **178**, 416 (1986).

[2] J. Schukraft, "Heavy Ion Physics at the LHC: What's new ? What's next ?", arXiv:1311.1429 [hep-ex].

[3] L. Kluberg and H. Satz, "Color Deconfinement and Charmonium Production in Nuclear Collisions," arXiv:0901.3831 [hep-ph].

[4] N. Brambilla, S. Eidelman, B. K. Heltsley, R. Vogt, G. T. Bodwin, E. Eichten, A. D. Frawley and A. B. Meyer *et al.*, "Heavy quarkonium: progress, puzzles, and opportunities," Eur. Phys. J. C **71**, 1534 (2011).

[5] A. Adare *et al.* [PHENIX Collaboration], "J/ψ suppression at forward rapidity in Au+Au collisions at $\sqrt{s_{NN}} = 200$ GeV," Phys. Rev. C **84**, 054912 (2011).

[6] A. Andronic, P. Braun-Munzinger, K. Redlich and J. Stachel, "Statistical hadronization of charm in heavy ion collisions at SPS, RHIC and LHC," Phys. Lett. B **571**, 36 (2003).

[7] H. L. Lai, M. Guzzi, J. Huston, Z. Li, P. M. Nadolsky, J. Pumplin and C.-P. Yuan, "New parton distributions for collider physics," Phys. Rev. D **82**, 074024 (2010), [arXiv:1007.2241 [hep-ph]].

[8] S. Chatrchyan *et al.* [CMS Collaboration], "J/ψ and ψ_{2S} production in pp collisions at $\sqrt{s} = 7$ TeV," JHEP **1202**, 011 (2012) [arXiv:1111.1557 [hep-ex]].

[9] V. Khachatryan *et al.* [CMS Collaboration], "Measurement of J/ψ and ψ(2S) Prompt Double-Differential Cross Sections in pp Collisions at $\sqrt{s}$=7TeV," Phys. Rev. Lett. **114**, no. 19, 191802 (2015), [arXiv:1502.04155 [hep-ex]].

[10] G. Aad *et al.* [ATLAS Collaboration], "Measurement of the differential cross-sections of prompt and non-prompt production of J/ψ and ψ(2S) in pp collisions at $\sqrt{s} = 7$ and 8 TeV with the ATLAS detector," arXiv:1512.03657 [hep-ex].

[11] R. Baier and R. Ruckl, "Hadronic Collisions: A Quarkonium Factory," Z. Phys. C **19**, 251 (1983).

[12] B. Humpert, "Narrow Heavy Resonance Production By Gluons," Phys. Lett. B **184**, 105 (1987).

[13] R. Gastmans, W. Troost and T. T. Wu, "Production of Heavy Quarkonia From Gluons," Nucl. Phys. B **291**, 731 (1987).

[14] P. L. Cho and A. K. Leibovich, "Color octet quarkonia production," Phys. Rev. D **53**, 150 (1996), [hep-ph/9505329].

[15] P. L. Cho and A. K. Leibovich, "Color octet quarkonia production. 2.," Phys. Rev. D **53**, 6203 (1996), [hep-ph/9511315].

[16] E. Braaten, S. Fleming and A. K. Leibovich, "NRQCD analysis of bottomonium production at the Tevatron," Phys. Rev. D **63**, 094006 (2001), [hep-ph/0008091].

[17] E. J. Eichten and C. Quigg, "Mesons with beauty and charm: Spectroscopy," Phys. Rev. D **49**, 5845 (1994) [hep-ph/9402210].

[18] R. Sharma and I. Vitev, "High transverse momentum quarkonium production and dissociation in heavy ion collisions," Phys. Rev. C **87**, no. 4, 044905 (2013), [arXiv:1203.0329 [hep-ph]].

[19] M. Butenschon and B. A. Kniehl, "Reconciling J/ψ production at HERA, RHIC, Tevatron, and LHC with NRQCD factorization at next-to-leading order," Phys. Rev. Lett. **106**, 022003 (2011).

[20] M. Butenschoen and B. A. Kniehl, "World data of J/psi production consolidate NRQCD factorization at NLO," Phys. Rev. D **84**, 051501 (2011).

[21] M. Butenschoen and B. A. Kniehl, "Probing nonrelativistic QCD factorization in polarized J/ψ photoproduction at next-to-leading order," Phys. Rev. Lett. **107**, 232001 (2011).

[22] D. Acosta *et al.* [CDF Collaboration], "Measurement of the J/ψ meson and $b-$hadron production cross sections in $p\bar{p}$ collisions at $\sqrt{s} = 1960$ GeV," Phys. Rev. D **71**, 032001 (2005).

[23] F. Abe *et al.* [CDF Collaboration], "Production of J/ψ mesons from χ_c meson decays in $p\bar{p}$ collisions at $\sqrt{s} = 1.8$ TeV," Phys. Rev. Lett. **79**, 578 (1997).

[24] K. Nakamura *et al.* [Particle Data Group Collaboration], "Review of particle physics," J. Phys. G **37**, 075021 (2010).